ELSEVIER

Journal of Power Sources 113 (2003) 131–144

JOURNAL OF POWER SOURCES

www.elsevier.com/locate/jpowsour

# Modelling static and dynamic behaviour of proton exchange membrane fuel cells on the basis of electro-chemical description

M. Ceraolo[a,*], C. Miulli[a], A. Pozio[b]

[a]*Department of Electrical Systems and Automation, University of Pisa, Via Diotisalvi 2, Pisa 56126, Italy*
[b]*Department of Energy ENEA, Italian Agency for New Technologies, Energy and the Environment, Pisa 56126, Italy*

Received 6 December 2001; received in revised form 11 July 2002; accepted 23 September 2002

**Abstract**

A simplified dynamical model of a fuel cell of the proton exchange membrane (PEM) type, based on physical–chemical knowledge of the phenomena occurring inside the cell has been developed by the authors.

The model has been implemented in the MATLAB/SIMULINK environment.

Lab tests have been carried out at ENEA's laboratories; and a good agreement has been found between tests and simulations, both in static and dynamic conditions.

In a previous study [M. Ceraolo, R. Giglioli, C. Miulli, A. Pozio, in: Proceedings of the 18th International Electric Fuel Cell and Hybrid Vehicle Symposium (EVS18), Berlin, 20–24 October 2001, p. 306] the basic ideas of the model, as well as its experimental validation have been published.

In the present paper, the full implementation of the model is reported in detail. Moreover, a procedure for evaluating all the needed numerical parameters is presented.



*Keywords:* Fuel cell; Modelling; Simulation

## 1. Introduction

The need of reducing pollutant emissions and of utilising more efficiently the available energy resources (in particular fossil resources) has caused, in recent years, an ever increasing attention towards fuel cells. In fact, their high conversion efficiency and low environmental impact, make them good candidates for substituting, at least in some applications, more conventional conversion systems.

One of the applications of fuel cells currently being considered is as a source of energy for electric vehicles, normally in hybrid configuration.

Among the several possible kinds of fuel cells, the polymer electrolyte fuel cells (PEFCs), also called proton exchange membrane fuel cells (PEMFCs), appear to be the best candidate for the use aboard of electric vehicles in which simplicity, high specific power, rapid start-up (even at low temperature) have the maximum importance [4,11,16].

To be able to utilise these devices in an effective way, it is, however, mathematical models of the vehicle fuel cell stack are necessary so that the system behaviour can be analysed at the design stage by means of computer simulations in different conditions of load, pressure of reagent gases, temperature.

These models can be integrated with other components in vehicle simulation environments (such as the one described in [17]), so that the whole system of a fuel cell vehicle can be analysed in detail.

Several mathematical model of PEM fuel cells have already been presented [4–12]. The majority of them, however, is able to simulate only the cell steady-state behaviour, while the analysis of their performance in dynamic conditions is important for the use aboard of vehicles, given the rapid variation of mechanical and electrical quantities.

Some models [7,11] are characterised by a high complexity, with several partial differential equations to be kept into account. This high complexity creates problems of simulation times, parameter identifications, etc. especially when they are to be enclosed into a larger system, such as the electric vehicle.

The purpose of this paper, therefore, is to propose a dynamical model of PEM fuel cells that, although simplified and containing some empirical equations, is still based on

* Corresponding author. Tel.: +39-50-565305; fax: +39-50-565333.
*E-mail address:* ceraolo@dsea.unipi.it (M. Ceraolo).

0378-7753/02/$ – see front matter 
PII: S0378-7753(02)00565-7

**Nomenclature**

| | |
|---|---|
| $A_r$ | effective Pt surface area per unit geometric surface area ($cm^2/cm^2$) |
| $A_{ro}$ | total Pt surface area per unit geometric surface area ($cm^2/cm^2$) |
| $b$ | Tafel slope (V) |
| $c_{H^+}$ | dimensionless proton concentration |
| $c_k$ | concentration of species $k$ ($mol/cm^3$) |
| $C_{dl}$ | double-layer capacitance ($F/cm^2$) |
| $\mathscr{D}_{ik}$ | total pressure-diffusivity product (bar $cm^2/s$) |
| $D_{ik}$ | diffusivity of the gas pair $i$–$k$ ($cm^2/s$) |
| $E_o$ | open-circuit voltage (V) |
| $E_{oC}$ | cathode potential (V) |
| $E_{ref}$ | reference voltage (V) |
| $f$ | frequency ($s^{-1}$) |
| $F$ | Faraday's constant (96484 C/eq.) |
| $[H^+]$ | proton concentration ($mol/cm^3$) |
| $j$ | cell current density ($A/cm^2$) |
| $j_o$ | exchange current density ($A/cm^2$) |
| $j_r$ | reaction density current ($A/cm^2$) |
| $L_d$ | thickness of diffusion layer (cm) |
| $N_{air}$ | inlet air mole flow ($mol/(cm^2\ s)$) |
| $N_{H_2}$ | hydrogen consumption ($mol/(cm^2\ s)$) |
| $N_k$ | superficial flux of species $k$ ($mol/(cm^2\ s)$) |
| $N_{1dc}$ | oxygen flux at interface diffusion layer–catalyst layer ($mol/(cm^2\ s)$) |
| $p_c$ | cathode total pressure (atm) |
| $p_k$ | partial pressure of species $k$ (bar) |
| $p_{1c}$ | oxygen partial pressure within catalyst layer (bar) |
| $p_{1o}$ | zero-current oxygen partial pressure (bar) |
| $R$ | gas constant (82.056 (bar $cm^3$)/(K mol) = 8.3144 J/(K mol)) |
| $R_{ohm}$ | internal ohmic resistance (ohm $cm^2$) |
| $T$ | absolute temperature (K) |
| $x_k$ | mole fraction of species $k$ |
| $y$ | distance through diffusion layer (cm) |

*Greek letters*

| | |
|---|---|
| $\beta$ | inlet nitrogen–oxygen mole ratio |
| $\varepsilon_g$ | porosity of diffusion layer |
| $\Delta\phi_{ce}$ | catalyst–electrolyte potential difference (V) |
| $\eta$ | cathode overpotential (V) |
| $\tau$ | tortuosity of diffusion layer |
| $\tau_{H^+}$ | time constant of proton concentration (s) |
| $\xi$ | dimensionless distance |

the chemical–physical knowledge of the phenomena occurring inside the cell.

The effort carried-out was to simplify as much as possible the analytical aspects, so that simulation and numerical parameter identification are eased.

The model is implemented in the well known and highly widespread simulation environment MATLAB/SIMULINK.

## 2. Mathematical definition of the proposed model

### 2.1. A simple description of the cell structure

A PEM fuel cell is constituted by a membrane able to conduct protons disposed between two electrodes. The electrodes-membrane assembly, in turn, is pressed by two conductive plates containing some channels in which the reactants flow.

A simplified representation of the cell is reported in Fig. 1. The main elements composing the cell are: conductor plates, electrodes and membrane.

The electrodes are constituted by a *gas diffusion layer* (made of carbon paper or cloth, carbon powder and PTFE) and a *catalyst layer* (constituted by Pt/C powder and Nafion ionomer); both have a porous, partially hydrophobic, structure.

According to several studies [3–11], the larger pores (called *macropores*) operate as a ducts for the reactants from the flow channels towards the catalyst layer, while the smaller ones (*micropores*) operate as a ducts for the passage of water.

The reactions occurring in the catalytic layer of the electrodes are the following ones: at the anode the hydrogen decomposes and yields electrons to platinum and protons to the membrane:

$$H_2 \rightarrow 2H^+ + 2e^- \tag{1}$$

at the cathode, the oxygen reacts with the protons coming from the membrane and with the electrons supplied by the catalyst and forms molecules of water:

$$\tfrac{1}{2}O_2 + 2H^+ + 2e^- \rightarrow H_2O. \tag{2}$$

The membrane, if well humidified, has a proton conductivity sufficiently high.

Inside the cells, however, because of the dragging of water molecules by the proton flow, the part of the membrane on the cathode side tends to saturate, while the one on the anode side tend to dehydrate, with a consequent conductivity reduction; to limit this phenomenon, and to avoid water loss by evaporation, the cell is fed with humidified gases at higher temperatures than the cell temperature.

### 2.2. The cell voltage versus current density behaviour

The PEM fuel cell behaviour is quite complex and is influenced by several factors, including composition and structure of electrodes and membrane type.

An analysis of a large amount of experimental data reported in literature [7,11,14,23–25] has shown that the voltage versus current density plots for a PEM cell have a behaviour of the type shown in Fig. 2, in which the numerical values are quite typical although, obviously, the actual values of any particular cell can differ from them.

Since the early 1960s, a lot of papers have been published on the modelling of PEM cells. The objectives of these studies were to analyse the effects of composition and

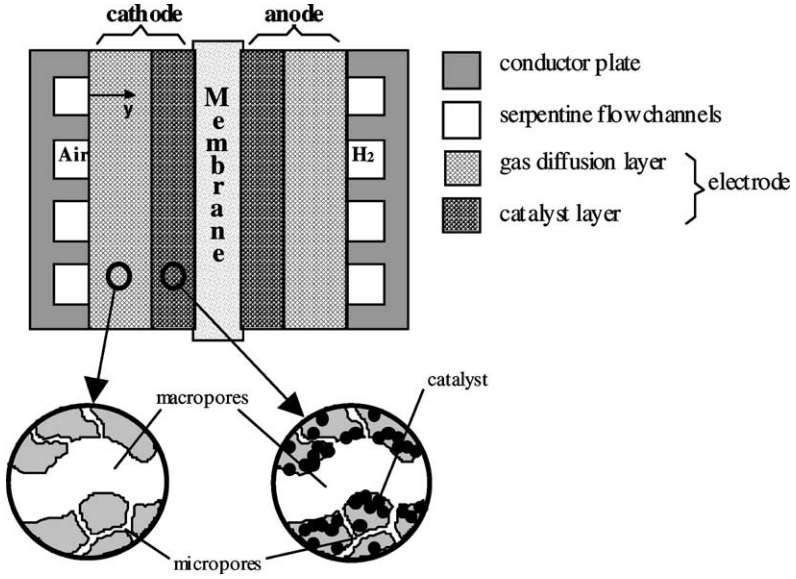


Fig. 1. Schematic representation of a PEM fuel cell, showing the internal structure of electrodes.

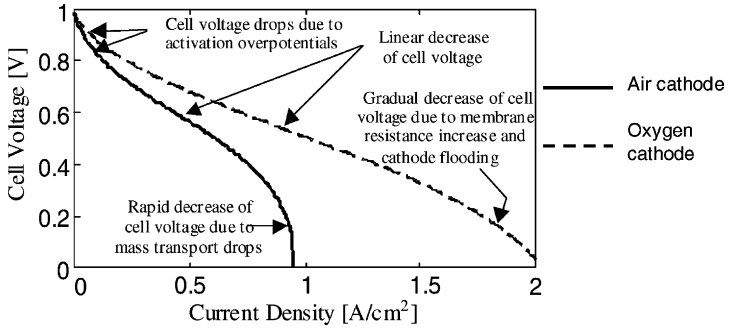


Fig. 2. Typical cell voltage vs. current density plots for PEM fuel cells and a common interpretation for the voltage drop.

structure of cell on the cell or half-cell voltage versus current density behaviour [9].

Initially, less attention was given to cathode problems than was devoted to ionomeric membranes. This initial emphasis on voltage drops in the membrane electrolyte was required because this unique component of cell is quite different from the electrolytes employed in other low-temperature fuel cell types [7]. With the development of membrane and particularly with the introduction of thinner types, it has become clear that voltage drops in membrane of a well-humidified PEM cell are not always the prevalent ones, particularly in cells with air as oxidant. With membranes as Nafion 112 (50 μm thickness), Membrane Dow (80 μm thickness), Membrane "C" (140 μm thickness), the cell resistance in well-humidified PEM cells does not increase excessively with the current, even at densities as high as 2.5–3 A/cm$^2$ [7,14].

According to the already mentioned literature, the voltage drops in a PEM fuel cell can originate from

1. *limited cathode interfacial kinetics*, which determines high voltage drops mainly in low current density region (Fig. 2), both with air and oxygen cathode;
2. *limited protonic conductivity* in the catalyst layer and in the membrane electrolyte; in the case of oxygen cathode the ohmic drops within the membrane constitute the major fraction of measured drops in the current range of interest;
3. *anode interfacial kinetics*, which determines a voltage drop linear with the current density because of the high exchange current density for the electrooxidation of hydrogen; however, these drops result to be very small when compared to the others;
4. *limited cathode mass transport*, particularly in the case of air cathode, which determines a rapid decrease of cell voltage with current density; this diffusion limitation lead to pseudo resistive effects at moderate current densities and the appearance of limiting currents at high current densities;
5. *cathode*"*flooding*", when the water produced from cathode reaction is not removed effectively from the cell; consequently the excess liquid water leads to a poor transport of oxygen through the electrode; this phenomenon, with optimised cells, occurs typically in oxygen cathode at very high current densities, which cannot be reached if the cell cathode is fed with air.

### 2.3. Basic assumptions and model structure

The model considers a cell that utilises $H_2$ as a fuel and air as oxidant, both humidified.

Based on the basic considerations reported in the previous section, the main assumptions of the proposed model are as follows:

1. The electrode (diffusion and catalyst) layers have been considered as having given, and constant porosity and tortuosity. This implies that the possibility of cathode flooding is not considered, since it would change the size of macropores and therefore the layer effective porosity.
2. The model is one-dimensional, i.e. all quantities vary only in the direction orthogonal to anode and cathode surfaces.
3. The temperature is supposed to be uniform in the cell.
4. As often made by authors [5–10] the air total pressure is assumed to be uniform, while the variation with space of the partial pressures of its components is kept into account. As a consequence of this, the movement of gases within electrodes is consequence of just concentration and not pressure gradients.
5. The water vapour contained in the reactants of the baking macropores is in equilibrium with the surrounding liquid phase; consequently the partial water pressure is uniform.
6. The membrane is considered as being completely saturated of water; therefore, its conductivity is only function of temperature.
7. The anodic overpotential is disregarded with respect to the cathode ones (cf. [7,8,16]); consequently, the voltage across the anode is considered to be constant.

According to these assumptions, the proposed mathematical model is composed by the elements shown in Fig. 3, in which also the logical connections of the different blocks, and the model inputs and outputs are shown.

In the following paragraphs, a description of the implementation of the different blocks of Fig. 3 is reported making reference, as usual, to current densities instead of actual cell and reaction current.

### 2.4. Cathode gas diffusion

The oxygen contained in the air entering the cell before reaching the catalyst layer diffuses, through the diffusion layer, within a gaseous mix constituted by nitrogen, water vapour and the oxygen itself, all considered as being ideal gases. This phenomenon is described [5,8] by the following differential equations:

*continuity equations*:

$$\frac{\varepsilon_g}{RT}\frac{\partial p_i}{\partial t} + \frac{\partial N_i}{\partial y} = 0 \tag{3}$$

*Stefan–Maxwell equations of diffusion*:

$$\frac{\varepsilon_g}{\tau^2}\frac{\partial p_i}{\partial y} = \sum_{k=1}^{3} \frac{RT}{p_c \mathscr{D}_{ik}}(p_i N_k - p_k N_i), \tag{4}$$

where $i, k \in (1, 3)$ and $p_1$ is the oxygen partial pressure, $p_2 = p_{sat}(T)$ the water vapour partial pressure, $p_3$ the nitrogen partial pressure and $p_c \mathscr{D}_{ik} = D_{ik} = D_{ik}(T)$, in which $p_c = p_1 + p_2 + p_3$ is the cathode (air) pressure, assumed, in accordance to hypothesis 4 stated in Section 2.3, constant.

The analytical expressions of the diffusivities $D_{ik}(T)$ have been taken from [13].

The diffusion layer porosity $\varepsilon_g$ (ratio between pore volume and total layer volume) is considered independent on the cell operating conditions; the parameter $\tau$ (tortuosity: ratio

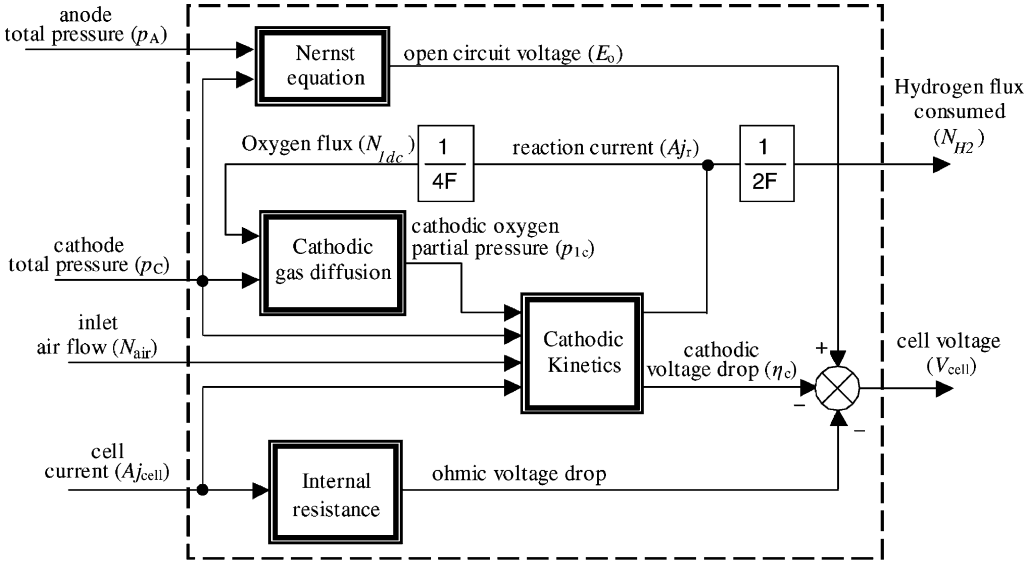


Fig. 3. The general model structure.

between actual pore length and macroscopic diffusion layer thickness) keeps into account the fact that the distance the oxygen covers for reaching the catalytic layer is greater than the diffusion layer thickness, because of the pore curvature.

Combining Eqs. (3) and (4) and applying the hypotheses stated in the previous paragraph, the following single partial differential equation can be obtained, having the unique unknown $p_1$ (oxygen partial pressure):

$$\frac{\partial p_1}{\partial t} = \omega \frac{\partial^2 p_1}{\partial \xi^2} - \psi \frac{j_r}{4F} \frac{\partial p_1}{\partial \xi} \tag{5}$$

in which $\xi$ is the dimensionless abscissa $y/L_d$, the variable $N_{1dc}$ is the oxygen flow at the interface diffusion-catalyst layers, and $\omega$ and $\psi$ are function of cell temperature and air pressure only:

$$\omega = \frac{1}{\tau^2 L_d^2((p_{sat}/D_{12}) + (p_c - p_{sat})/D_{13})},$$
$$\psi = \frac{RT}{\varepsilon_g L_d (p_c - p_{sat})}. \tag{6}$$

In Appendix A, mathematical details of the analysis by which Eq. (5) is derived are presented.

### 2.5. Cathode kinetics

The electrochemical reaction that occurs in the catalyst layer is the (2), in which the oxygen reacts with the protons present in the electrolyte and with the electrons supplied by the catalyst, thus forming water molecules.

The current that is created by the electrochemical reaction, in addition to the reactants concentration, depends on the potential difference between catalyst and electrolyte, as described by the Butler–Volmer equation [9,11]:

$$j_r = j_o A_r \left\{ \frac{p_1}{p_{1o}} \frac{[H^+]}{[H^+]_o} \exp\left(\frac{\eta}{b}\right) - 1 \right\} \tag{7}$$

$$\eta = E_{oC} - \Delta\phi_{ce} = E_o - V_{cell} - R_{ohm} j. \tag{8}$$

The cell current density, in turn, is the sum of the reaction current plus the contribution due to the charge storage in the electrical double-layer at the interface between catalyst and diffusion layers:

$$j = j_r + C_{dl} \frac{\partial \eta}{\partial t} \tag{9}$$

the double-layer capacitance $C_{dl}$ is assumed to be constant [16].

Some previous studies [5,6,11,12] have shown that the quantity of platinum interested by the chemical reaction lowers as the cell current rises; i.e. the reaction tends to concentrate in a smaller region of the catalyst layer, particularly when the cell is fed with air. This has been attributed to the limited electrolyte conductivity and limited oxygen transport that determine voltage drop and $O_2$ concentration gradient respectively.

To keep into account this phenomenon, without introducing a large number of partial-derivative differential equations, the parameter $A_r$ (ratio between total catalytic surface and cell surface) has been considered to be function of the cell current density, according to the following equation:

$$A_r = A_{ro} \exp(-a_1 j - a_2 j^5) \tag{10}$$

in which

$$a_1 = a_{1,ref} p_{O_2}^{\alpha_1} N_{air}^{\alpha_2} \exp\left(\frac{k_1}{T} - \frac{k_1}{T_{ref}}\right),$$
$$a_2 = a_{2,ref} \frac{p_{sat}}{p_c} N_{air}^{\alpha_3} \exp\left(\frac{k_2}{T} - \frac{k_2}{T_{ref}}\right). \tag{11}$$

The proposed expressions of $a_1$ and $a_2$ have been defined to interpolate at best the experimental results obtained at different temperatures and pressures of the reactant gases (see Section 3.4). Eqs. (10) and (11) are an empirical mathematical way to overcome the high computational complexity of the partial differential equations required to model the above-mentioned phenomenon.

In addition to (10), the variables that appear in (7) are considered to be functions of time only.

From experimental measures related to the reduction of oxygen in an acid environment [1,2] it is known that parameters $b$ and $j_o$ of (7) present a sudden rise for values of cathode voltage of about 0.80 V.

In [1], quantitative data on temperature dependence of electrode kinetics of oxygen reduction at platinum/Nafion interface are reported. All of the Tafel plots reported show two distinct slopes at all temperatures investigated and the break in the plots occurs at a potential of 0.75–0.8 V. This break has been observed previously and interpreted as a change in oxygen reduction mechanism [2]. The low Tafel slope, corresponding to a potential regime where oxygen reduction proceeds on Pt-oxide covered surface, results dependent on temperature according to the following relation

$$b_l = \frac{RT}{\alpha n F} \tag{12}$$

where $\alpha = 1$ and $n = 1$ has been assumed.

The high Tafel slope, corresponding to a potential regime where oxygen reduction proceeds on free-oxide Platinum, does not show a monotone behaviour with the temperature and can be considered temperature independent; from experimental data reported in [1] with the temperature changing from 30 to 80 °C the following constant value can be obtained:

$$b_h = 0.0504\,\text{V}. \tag{13}$$

The exchange current density $j_o$ shows a dependence both on temperature and oxygen partial pressure, and as the Tafel

slope, at high current densities it assumes different values from ones at low current densities.

To keep into account in the model of above-mentioned behaviour of the Tafel slope and the exchange current density, the two parameters ($b$ and $j_o$) has been defined as a function of the cathode overpotential $\eta$:

$$j_o = [j_{ol} + \Delta j \cdot u(\eta - \eta_b)] \tag{14}$$

$$b = b_l + (b_h - b_l) \cdot u(\eta - \eta_b) \tag{15}$$

in which $u(\,)$ is the Heaviside function and

$$\eta_b = E_0 - 0.8 \tag{16}$$

$$\Delta j = j_{ol}\left[\exp\left(\frac{\eta_b}{b_l} - \frac{\eta_b}{b_h}\right) - 1\right] \tag{17}$$

the overpotential $\eta_b$ is the cathode overpotential corresponding to break point in the Tafel plots on oxygen reduction at platinum/Nafion interface.

The $\Delta j$ expression in (17) has been obtained imposing the continuity of (7) with $\eta = \eta_b$.

Considering Eqs. (10), (14) and (17), the product $j_o A_r$ that appears in (7) becomes:

$$j_o A_r = j_{ol} A_{ro}\left\{1 + \left[\exp\left(\frac{\eta_b}{b_l} - \frac{\eta_b}{b_h}\right) - 1\right] \cdot u(\eta - \eta_b)\right\} \times \exp(-a_1 j - a_2 j^5) \tag{18}$$

in which, as shown also in literature [5,6], the product $j_{ol}A_{ro}$ results to be function of temperature and oxygen partial pressure:

$$j_{ol} A_{ro} = j_{ref} \exp\left(-\frac{k_o}{T} + \frac{k_o}{T_{ref}}\right) p_{O_2}^{\alpha_o}. \tag{19}$$

Differently from what assumed in other papers [4,6,9,11], the proton concentration $[H^+]$ in the catalyst layer has been considered to be a function of the cell current. This because if the cell current rises the water production and the hydration of the polymeric electrolyte near the cathode catalyst tend to rise as well, causing this way an increase in the number of mobile protons. In fact, from experimental data [15], it is known that the proton conductivity of a polymer electrolyte increases with the water content in the polymer, and this behaviour is attributed to the increase of the number if mobile protons with the water content.

For a polymer electrolyte the conductivity is defined as [5,10]:

$$\sigma = \frac{F^2}{RT} D_{H^+} c_{H^+} \tag{20}$$

so if it increases with the water content the proton concentration increases as well, according to (20).

This hypothesis is able to explain the voltage overshoot visible in the cell experimental response to sudden current reductions (Fig. 4), that was already observed in [18] without explanations: if the cell current increases very fast the proton concentration near the cathode catalyst increases very fast as well, while if the cell current decreases very fast the proton concentration decreases more slowly following the slow dynamics of the excess water removal from the cathode catalyst layer.

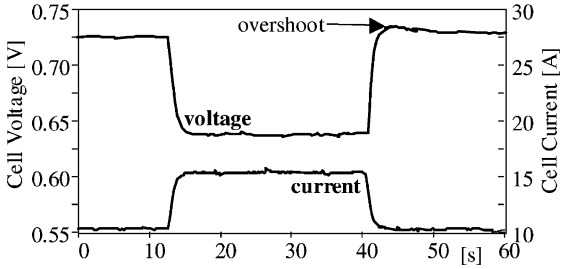


Fig. 4. Cell dynamic response to a current step.

Therefore, the behaviour over time of the proton concentration $[H^+]$ has been defined by the following empirical differential equation:

$$u\left(-\frac{\partial c_{H^+}}{\partial t}\right) \cdot \frac{\partial c_{H^+}}{\partial t} + \frac{c_{H^+}}{\tau_{H^+}} = \frac{1 + \alpha_{H^+} \cdot j^3}{\tau_{H^+}} \tag{21}$$

in which $u(\,)$ is the Heaviside function, $C_{H^+} = [H^+]/[H^+]_o$ the dimensionless proton concentration, $\tau_{H^+}$ the time constant related to the $C_{H^+}$ dynamics, and $\alpha_{H^+}$ is a parameter that links $C_{H^+}$ to the cell current.

### 2.6. Internal resistance and voltage drops

The passage of current through the cell causes ohmic voltage drops basically due to the electron transfer in electrodes and in the conductive graphite plates and to the proton transfer through the membrane.

Since the conductivity of graphite is much larger than the one of the membrane [4,12], the drops due to the electron transfer can be neglected; therefore, the cell internal resistance practically coincides with that of membrane.

In general, the membrane resistance results to be a function, in addition of temperature, also of the current [14,15]. As shown in some previous studies related to the simulation of the Nafion membrane behaviour [20,21], when the current rises the dragging from anode to cathode of water molecules by the current causes a rising concentration gradient. As a consequence, the side of the membrane on the cathode and anode parts tends to saturate and dehydrate respectively, with a reduction of the local conductivity and an increase in the membrane resistance. This phenomenon, with optimised cells, occurs typically in oxygen cathode at very high current densities, which cannot be reached if the cell is fed with air.

As far as the influence of temperature on membrane conductivity, it can be said that, for temperatures below 100 °C, if the temperature increases the conductivity increases as well.

In [15], experimental data on the temperature dependence of proton conductivity of some membranes are reported. The tested membranes were Nafion 117, "C" Membrane and Dow Membrane, and their conductivity was determined

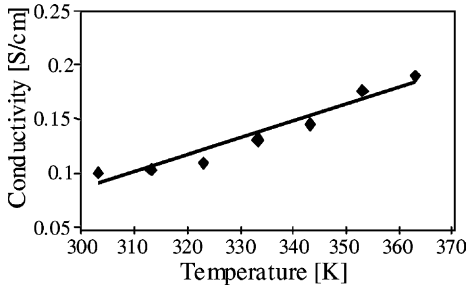


Fig. 5. Proton conductivity of Nafion 117 immersed in water (from [15]).

both with membranes immersed in water and with membranes partially hydrated. All membranes immersed in water showed a quite linear behaviour of the conductivity with the temperature over the range 30–90 °C. In Fig. 5, conductivity values of Nafion 117 are reported.

In [22], the proton conductivity of Nafion 117 was measured under various conditions of humidity and temperature, and all measures were carried out with the membrane under exposure to a stream of humid gas. The conductivity measured at different temperatures exhibited a behaviour as shown in Fig. 6. In this case, the conductivity has not a monotone behaviour with the temperature, but from 20 to 45 °C it decreases and then it increases when the temperature increases from 45 to 80 °C. This behaviour was attributed to the decrease of water content in the membrane between 20 and 45 °C, considering that above 45 °C the water content was rather constant.

From the experimental observations made by the ENEA's labs related to a PEM cell having a Nafion 115 membrane, the internal resistance resulted to be, in practice, function of only temperature in the range from 40 to 80 °C. In Figs. 7 and 8, some values of cell resistance at 60 and 70 °C are reported. The resistance was determined as high frequency value of cell impedance for small ac signal around steady-state current values (Section 3.2). As shown in the figures the resistance resulted to be independent on gas pressures; moreover, as the temperature changes, the behaviour of resistance versus current may switch from decreasing to increasing.

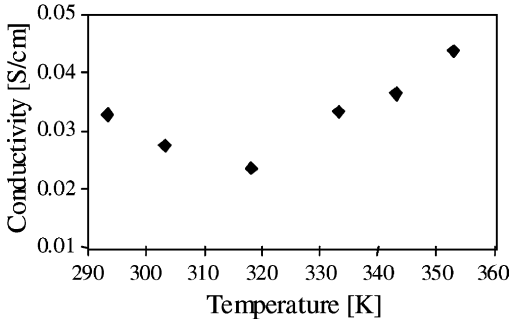


Fig. 6. Proton conductivity of Nafion 117 under exposure to a stream of humid gas (from [22]).

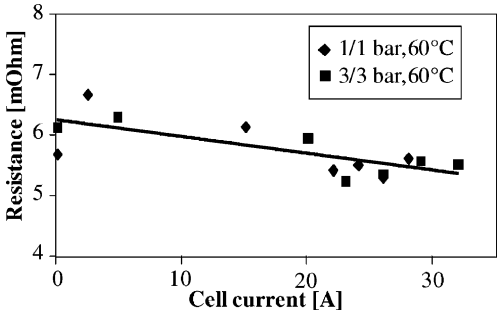


Fig. 7. Internal resistance at 60 °C and different pressures of reactant gas.

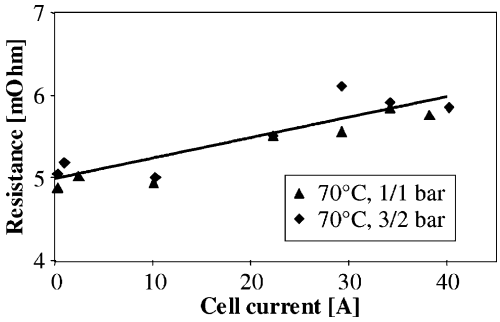


Fig. 8. Internal resistance at 70 °C and different pressures of reactant gas.

As a consequence, for sake of simplicity, at each temperature the cell resistance was chosen as the average of all values obtained at the different currents and gas pressures.

In Fig. 9, the resistance values determined in the range from 40 to 80 °C are reported; in the model they have been interpolated by the following equation:

$$R_{\text{ohm}} = R_{\text{ref}} + \alpha_T(T - T_{\text{ref}}) \quad (22)$$

in which $T_{\text{ref}} = 343.15$ K.

In Fig. 10, a comparison of conductivity values determined in this work with those reported in [22], and obtained with the membrane operating in conditions similar to those occurring in the actual cell, is shown.

The comparison shows a good agreement in terms of trend of conductivity with the temperature; the marked differences in terms of numerical values shown in Fig. 10 have little significance since important differences exist in the measure conditions of the two cases.

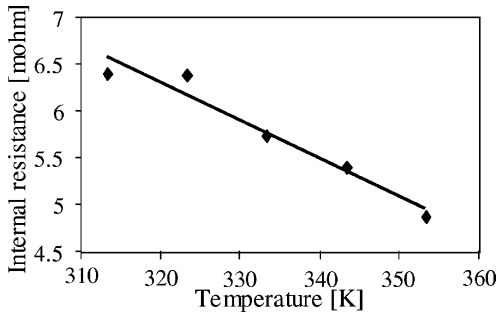


Fig. 9. Internal resistance at different temperatures.

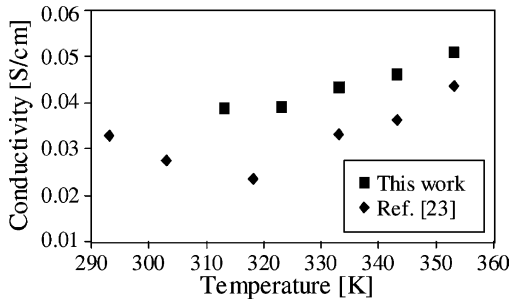


Fig. 10. Comparison between the conductivities utilised in this work and in [22].

### 2.7. Open-circuit voltage (OCV)

The open-circuit voltage has been defined by means of the Nernst equation

$$E_o = E_{ref} + \frac{dE_o}{dT}(T - T_{ref}) + \frac{RT}{2F}\ln(p_{H_2}p_{O_2}^{1/2}) \quad (23)$$

applied to cell reaction

$$H_2(g) + \tfrac{1}{2}O_2(g) \rightarrow H_2O(aq).$$

To improve agreement to the experimental results, the Eq. (23) is slightly modified as follows:

$$E_o = E_{ref} + \frac{dE}{dT}(T - T_{ref}) + k\frac{RT}{2F}\ln(p_{H_2}p_{O_2}^{1/2}) \quad (24)$$

in which the parameter $k$ has been introduced. In fact, with a $k$ of 1 and standard values of $E_{ref}$, $dE/dT$, the $E_o$ would be much higher than the values experimentally observed, as already noted in the past [1].

The reference temperature $T_{ref}$ has been fixed to 343.15 K.

### 2.8. Steady-state cell voltage

The simplifying assumption contained in Eq. (10) allows to derive an analytical expression able to fit the experimental data of cell voltage over the whole range of current.

The steady-state solution of Eq. (5) (Appendix A) gives the oxygen partial pressure in the diffusion layer as function of cell density current:

$$p_1(\xi) = p_{1o}[1 + \beta - \beta\exp(vj\xi)] \quad (25)$$

in which $v = \psi/4\omega F$ then the oxygen partial pressure in the catalyst layer ($\xi = 1$) will be

$$p_1(1) = p_{1o}[1 + \beta - \beta\exp(vj)]. \quad (26)$$

Combining Eqs. (7)–(9) and (26) the following analytical expression of the cell voltage can be obtained:

$$V_{cell} = E_o + b\ln(j_oA_{ro}) - (a_1j + a_2j^5) + b\ln\left\{\frac{[1 + \beta - \beta\exp(vj)](1 + \alpha_{H^+}j^3)}{j + j_oA_r}\right\} - R_{ohm}j. \quad (27)$$

This result can be obtained considering that, in steady-state conditions, $j_o$ and $b$ can be expressed as a function of $j$:

$$j_o = j_{ol} + \Delta j \cdot u(j - j_b), \qquad b = b_l + (b_h - b_l)\cdot u(j - j_b) \quad (28)$$

in which $j_b$ is the current density that, in steady-state, corresponds to $\eta_b$.

The Eq. (27) is used in this work to determine the parameters $j_{ol}$, $A_{ro}$, $a_1$, $a_2$ and $v$ as functions of cell temperature, gas pressures and gas flows (Section 3.4).

## 3. Identification of numerical values of parameters

The proposed model contains 22 numerical parameters that need to be identified; they are shown in Table 1, along with the equations in which they appear.

Among which, the parameters $\beta$ and $b_h$ can be directly found in literature ([5] and [1], respectively). In the following a possible procedure for determining all the other parameters of Table 1 is presented.

### 3.1. Open-circuit voltage (parameters $E_{ref}$, $dE_o/dT$, $k$)

The cell voltage stabilises completely after several seconds (a minute or so) from any change in the parameters from the exterior, i.e. reactant pressures, cell temperature and/or current density.

If the OCV is measured for different values of $p_{H_2}$, $p_{O_2}$ and $T$, the three parameters $E_{ref}$, $dE_o/dT$, $k$ can be easily found using Eq. (24). In Table 2, some experimental values of OCV at different temperatures and pressures are reported.

Table 1
Numerical parameters of the model

| Parameter | Equation |
|---|---|
| $\tau L_d$ | (6) |
| $\varepsilon_g L_d$ | (6) |
| $\beta$ | (25) |
| $C_{dl}$ | (9) |
| $a_{1,ref}$ | (11) |
| $k_1$ | (11) |
| $\alpha_1$ | (11) |
| $\alpha_2$ | (11) |
| $a_{2,ref}$ | (11) |
| $k_2$ | (11) |
| $\alpha_3$ | (11) |
| $b_h$ | (15) |
| $j_{ref}$ | (19) |
| $k_o$ | (19) |
| $\alpha_o$ | (19) |
| $\tau_{H^+}$ | (21) |
| $\alpha_{H^+}$ | (21) |
| $R_{ref}$ | (22) |
| $\alpha_T$ | (24) |
| $E_{ref}$ | (24) |
| $dE_o/dT$ | (24) |
| $k$ | (24) |

Table 2
Variation of open-circuit voltage with temperature and pressures of reactants

| $T$ (°C) | $p_c$ (bar) | $p_a$ (bar) | $p_{O_2}$ (bar) | $p_{H_2}$ (bar) | OCV (V) |
|---|---|---|---|---|---|
| 70 | 1 | 1 | 0.143 | 0.680 | 0.959 |
| 70 | 2 | 1 | 0.349 | 0.680 | 0.966 |
| 70 | 3 | 2 | 0.556 | 1.667 | 0.978 |
| 70 | 4 | 3 | 0.763 | 2.654 | 0.984 |
| 50 | 3 | 2 | 0.594 | 1.851 | 0.985 |
| 30 | 3 | 2 | 0.611 | 1.930 | 0.989 |

Table 3
Numerical parameters of model

| Parameter | Unit | Value |
|---|---|---|
| $\tau L_d$ | cm | 0.149 |
| $\varepsilon_g L_d$ | cm | 0.026 |
| $\beta$ | – | 3.773 |
| $C_{dl}$ | mF/cm$^2$ | 41.71 |
| $a_{1,ref}$ | cm$^2$/A | 25,460 |
| $k_1$ | K | 1174 |
| $\alpha_1$ | – | 0.238 |
| $\alpha_2$ | – | 0.805 |
| $a_{2,ref}$ | (cm$^2$/A)$^5$ | 0.127 |
| $k_2$ | K | 20160 |
| $\alpha_3$ | – | −0.566 |
| $b_h$ | V | 0.0504 |
| $j_{ref}$ | A/cm$^2$ | $3.875 \times 10^{-3}$ |
| $k_o$ | K | 18300 |
| $\alpha_o$ | – | 0.583 |
| $\tau_{H^+}$ | s | 12.78 |
| $\alpha_{H^+}$ | (cm$^2$/A)$^3$ | 5.87 |
| $R_{ref}$ | Ω cm$^2$ | 0.269 |
| $\alpha_T$ | (Ω cm$^2$)/K | $2.02 \times 10^{-3}$ |
| $E_{ref}$ | V | 0.975 |
| $dE_o/dT$ | mV/K | 0.27 |
| $k$ | – | 0.755 |

The partial pressures of $O_2$ and $H_2$ have been determined considering at each temperature the water partial pressure.

The interpolation of experimental data by Eq. (24) yields the numerical values of parameters $E_{ref}$, $dE_o/dT$, $k$ reported in Table 3.

The Fig. 11 shows the comparison between experimental and calculated values after the fitting.

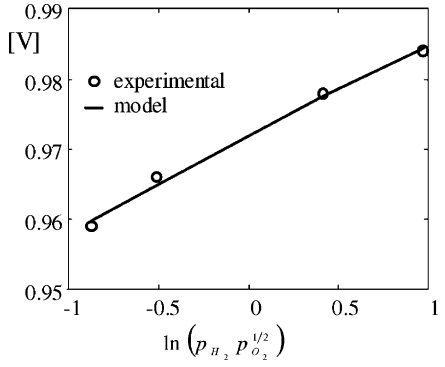


Fig. 11. Experimental and model values of open-circuit cell voltage at 70°C and different reactant pressures.

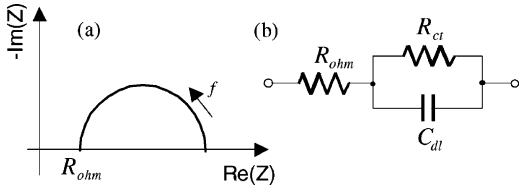


Fig. 12. (a) AC impedance spectrum at low overpotentials; (b) Equivalent circuit of ac impedance spectrum at low overpotentials.

### 3.2. Internal impedance (parameters $R_{ref}$, $\alpha_T$, $C_{dl}$)

If the cell is stimulated with small-amplitude signals at various frequencies a diagram of the complex impedance can be drawn in the Gauss plane.

Experimental results reported in [16] show that this impedance, while being described in detail with a two half-circle plot, is represented with sufficient precision with a single half-circle plot at small values of cathode over potential; this corresponds to an equivalent network for this impedance as shown in Fig. 12b.

In particular, the following tests can be carried out:

1. Tests at continuously increasing frequency (up to a few kHz) and a known cell temperature $T$ and gas pressures and small values of cathode overpotential (low currents); this allows to determine the value of $R_{ohm}$ as the value of the complex impedance at the left intercept of the half-circle with the real axis; it allows also the determination of $C_{dl}$ and $R_{ct}$: the experimental behaviour of the complex impedance $Z$ is to be replicated by the analytical equation:

$$Z(i\omega) = R_{ohm} + \frac{R_{ct}}{1 + i2\pi f R_{ct} C_{dl}},$$

where i is the imaginary unity.
2. Tests at different currents to determine the behaviour of $R_{ohm}$ with the current; the value of $R_{ohm}$ is determined as the left-intercept of measured impedance with the real axis.
3. Tests as those described in the previous two points, but at different temperatures and gas pressures to determine the dependence of $R_{ohm}$ and $C_{dl}$ on these two quantities. In this work, $R_{ohm}$ showed linear variation with temperature (Fig. 9), while the parameter $C_{dl}$ has not shown a monotone behaviour with the temperature and the gas pressures.

### 3.3. Parameters $\alpha_{H^+}$ and $\tau_{H^+}$

The parameters $\alpha_{H^+}$ and $\tau_{H^+}$ appear only in Eq. (21). If the cell is subjected to a sudden reduction in the cell current, the voltage behaviour is of the type shown in Fig. 13. In the figure, the part of the transient between $t_i$ and $t^*$ is dominated by the inner phenomena related to gas diffusion and double-layer space charge modifications.

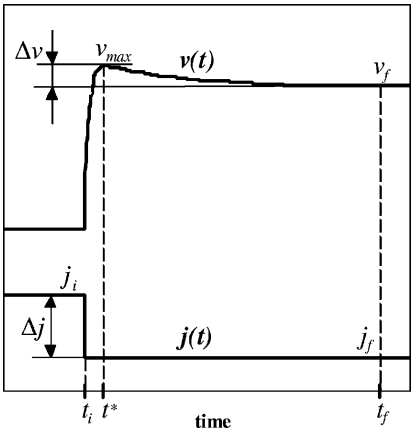


Fig. 13. Cell voltage response to a sudden current reduction.

Between $t^*$ and $t_f$, on the contrary, the phenomenon interpreted in the model as proton concentration variations is the major one. If this is assumed, in turn $b$ and $p_1$ can be assumed constant and it can be stated $j_r = j_f$, therefore,

$$j_r = j_f = j_o A_r \left\{ \frac{p_1 [H^+]}{p_{lo} [H^+]_o} \exp\left(\frac{\eta}{b}\right) - 1 \right\} \left( \frac{j_f}{j_o A_r} + 1 \right) \frac{p_{1o}}{p_1}$$
$$= \frac{[H^+]}{[H^+]_o} \exp\left(\frac{\eta}{b}\right) = \text{constant} = K.$$

If the cell is subjected to sudden current reductions of constant value $\Delta j$ and different final value $j_f$, a table can be built in which values of $\exp(\Delta v_k/b)$are associated to the corresponding values of $j_{f_k}$. The parameter $\alpha_{H^+}$ can be identified by interpolating the values $\exp(\Delta v_k/b)$ by means of the following function:

$$f(j_f) = \frac{1 + \alpha_{H^+} (j_f + \Delta j)^3}{1 + a_{H^+} j_f^3}. \tag{30}$$

Considering the Eq. (21), in the interval ($t^*$, $t_f$) the voltage behaviour is an exponential function having as time constant $\tau_{H^+}$. This time constant can therefore be inferred from the voltage behaviour as that shown in Fig. 13.

### 3.4. Parameters $\tau L_d$, $\varepsilon_g L_d$, $a_{1,ref}$, $k_1$, $\alpha_1$, $\alpha_2$, $a_{2,ref}$, $k_2$, $\alpha_3$, $j_{ref}$, $k_o$, $\alpha_o$

If steady-state voltage–current density curves are measured with different reactants pressures and temperatures, by means of an error minimisation function applied to Eq. (27), a set of numerical values can be found for each of the parameters $j_{ol}$, $A_{ro}$, $a_1$, $a_2$ and $v$.

Utilising these sets, in turn, by means of an error minimisation function applied to the equations reported in the left part of the following table, the numerical values of parameters reported in its right part can be determined:

| Equation | Parameters to be determined |
|---|---|
| $v = \frac{\psi}{4\omega F} = \frac{RT}{4F} \left[ \frac{p_{sat}}{(p - p_{sat}) D_{12}} + \frac{1}{D_{13}} \right] \frac{(\tau L_d)^2}{\varepsilon_g L_d}$ | $(\tau L_d)^2/\epsilon_g L_d$ |
| $a_1 = a_{1,ref} p_{O_2}^{a_1} N_{air}^{\alpha_2} \exp\left(\frac{k_1}{T} - \frac{k_1}{T_{ref}}\right)$ | $a_{1,ref}$, $k_1$, $\alpha_1$, $\alpha_2$ |
| $a_2 = a_{2,ref} \frac{p_{sat}}{p} N_{air}^{\alpha_3} \exp\left(\frac{k_2}{T} - \frac{k_2}{T_{ref}}\right)$ | $a_{2,ref}$, $k_2$, $\alpha_3$ |
| $j_{ol} A_{ro} = j_{ref} \exp\left(-\frac{k_o}{T} + \frac{k_o}{T_{ref}}\right) p_{O_2}^{\alpha_o}$ | $j_{ref}$, $k_o$, $\alpha_o$ |

Then,

$$\frac{[H^+]^*}{[H^+]_o} \exp\left(\frac{\eta^*}{b}\right) = \frac{[H^+]_f}{[H^+]_o} \exp\left(\frac{\eta_f}{b}\right),$$
$$\frac{[H^+]^*}{[H^+]_f} = \exp\left(\frac{\eta_f - \eta^*}{b}\right) = \exp\left(\frac{v_{max} - v_f}{b}\right) = \exp\left(\frac{\Delta v}{b}\right).$$

Finally, neglecting the proton concentration variation in the interval ($t_i$, $t^*$), it is

$$\frac{[H^+]^*}{[H^+]_f} = \exp\left(\frac{\Delta v}{b}\right) \cong \frac{[H^+]_i}{[H^+]_f} = \frac{1 + \alpha_{H^+} j_i^3}{1 + \alpha_{H^+} j_f^3}$$
$$= \frac{1 + \alpha_{H^+} (j_f + \Delta j)^3}{1 + \alpha_{H^+} j_f^3}. \tag{29}$$

Note that using just the steady-state cell behaviour it is not possible to separate $(\tau L_d)^2/\varepsilon_g L_d$ into its components $\tau L_d$ and $\varepsilon_g L_d$; this can be done instead by resorting to the dynamic cell behaviour, e.g. the response to a step current, by means of a trial and error procedure.

## 4. Comparison of simulated and measurement results

### 4.1. Experimental set-up and model parameter values

The cell under test, having a section of 50 $cm^2$, has been assembled at the ENEA's labs. The cathode had a catalyst E-TEK 20% Pt/C with 0.34 $mg/cm^2$ of Pt, while the anode

Table 4
Comparison between the values of some model parameters and corresponding values reported in literature

| $\tau L_d$ (cm) | $\varepsilon_g L_d$ (cm) | $C_{dl}$ (mF/cm$^2$) | $j_{ref}$ (mA/cm$^2$) | $L_d$ (cm) | $\tau$ | $\varepsilon_g$ | $T$ [°C] | Cathode Pt loading [mg/cm$^2$] | Ref. |
|---|---|---|---|---|---|---|---|---|---|
| 0.1490 | 0.0263 | 41.71 | 3.88 | – | – | – | 70 | 0.34 | This work |
| – | 0.0104 | – | $10^{-5}$ | 0.0260 | – | 0.40 | 80 | – | [6] |
| – | 0.0066 | – | 90.00 | 0.0300 | – | 0.22 | 80 | 0.12 | [7] |
| – | – | – | 10.80 | 0.0250 | – | – | 50–70 | 0.4 | [9] |
| 0.0850 | 0.0020 | – | $5.9 \times 10^4$ | 0.0170 | 5 | 0.12 | 80 | 0.10 | [11] |
| 0.2100 | 0.0120 | 13.70 | 32.80 | 0.0300 | 7 | 0.40 | 80 | 0.15 | [16] |

had a catalyst realised in laboratory with 20% Pt/C and 0.29 mg/cm$^2$ of Pt. The diffusion layer had 300 μm of thickness and the membrane was a Nafion 115 (125 μm).

The electrodes-membrane assembly has been pressed between two graphite plates provided with serpentine channels. Reactant gases were humidified Air and hydrogen.

In this section a comparison of simulated and measurement results is presented, both in steady-state and dynamic conditions.

The simulations are carried out with the presented model and the numerical values of the different parameters summarised in Table 3.

A comparison of values of all parameters in Table 3 to values of the same parameters which can be found in literature has not been possible; in fact the values found in literature has been only ones of the followings: $\tau L_d$, $\varepsilon_g L_d$, $C_{dl}$, $j_{ref}$ and $R_{ref}$.

In Section 2.6, a comparison has been done about the membrane conductivity and indirectly about the parameter $R_{ref}$.

In Table 4, a comparison about the other parameters is reported. As it can be seen, the values of parameters $\tau L_d$, $\varepsilon_g L_d$, $C_{dl}$, agree to ones reported in literature, while nothing can be said about the parameter $j_{ref}$, considering that its values reported in literature are in heavy disagreement among them.

### 4.2. Steady-state cell behaviour

The comparison is made both in steady state and dynamic conditions.

In Fig. 14, a comparison of steady-state experimental and simulated cell voltage under different operating conditions is reported.

The figure shows a good agreement of data, especially in the region of low densities (before the knee); this region is the one having the maximum interest for practical applications; a sufficient agreement is however present also even after the curve knees.

### 4.3. Dynamic cell behaviour

In Figs. 15 and 16, the dynamic response to current steps of the model is compared with the one experimentally measured, in different cell operating conditions.

In each case a good agreement is observed on the whole transient.

In particular in the case of Fig. 16, showing the response to an instantaneous interruption of the cell current, the agreement between experimental data and simulation is excellent.

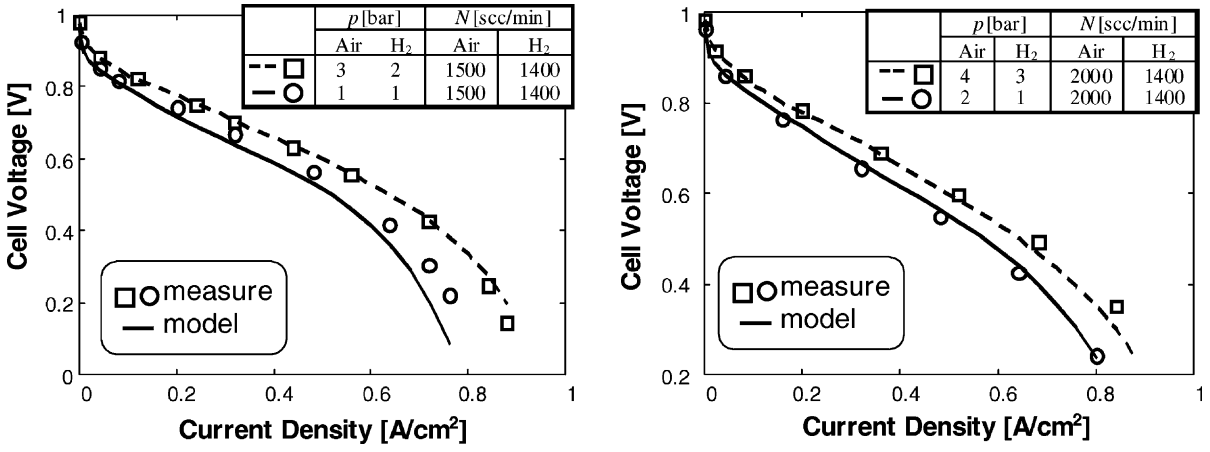


Fig. 14. Comparison of simulated and measured cell voltage at a cell temperature of 70 °C and different values of reactant pressures and flows.

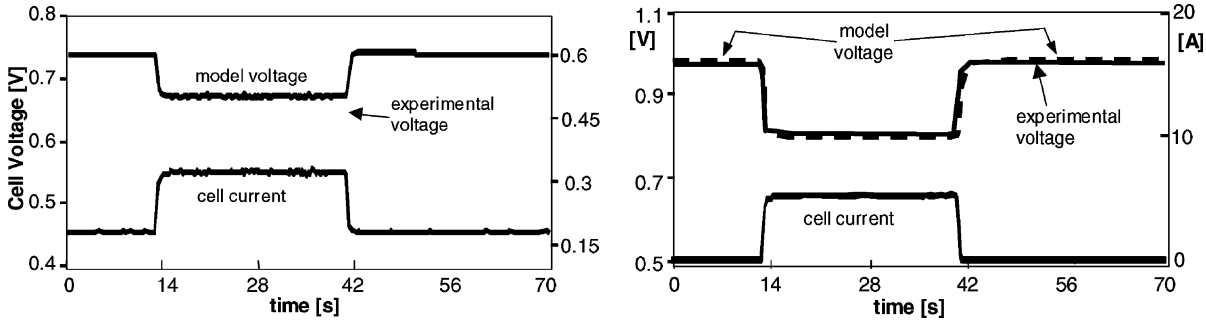


Fig. 15. Comparison of experimental and simulated cell dynamic response, considering two different current steps. Cell temperature 60 °C; reactant pressures 3 bar; air and $H_2$ flows 1000 and 500 scc/min respectively.

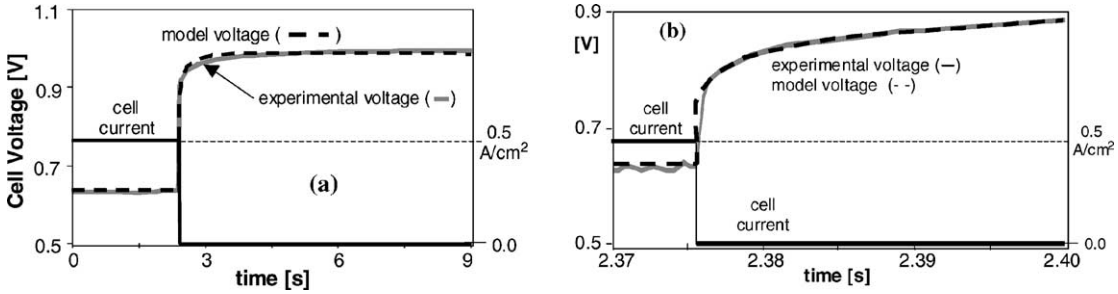


Fig. 16. Comparison of experimental and simulated cell dynamic response. Cell temperature 70 °C; air and $H_2$ pressures 3 and 2 bar; air and $H_2$ 1500 and 1400 scc/min, respectively. Part (b) is a zoom on a particular of figure (a).

## 5. Conclusion

A dynamical model of proton exchange membrane fuel cell, based on physical and chemical equations, has been proposed and described in detail.

A procedure for determining the numerical value of the 22 parameters for the proposed model has been proposed, the procedure has been applied to a real cell, and the values have been determined. A partial comparison of these values has been performed with similar results found in literature.

The behaviour of the proposed model, used with values of the numerical parameters found with the proposed identification procedure, has shown a good agreement with experimental results both in static and dynamic conditions.

This model is structured so that it can be easily extended to a whole stack of fuel cells.

It is believed that simplified versions of this model are to be derived, so that to avoid the presence of partial differential equations, and to reduce the number of parameters to be identified. Work is under way in this direction.

## Appendix A. Simplified equations for gas diffusion in cathode

The gas transport in cathode is described by the following equations considering air as an ideal gas (three-component gas):

*continuity equations*:

$$\varepsilon_g \frac{\partial c_1}{\partial t} + \frac{\partial N_1}{\partial y} = 0 \tag{A.1}$$

$$\varepsilon_g \frac{\partial c_2}{\partial t} + \frac{\partial N_2}{\partial y} = 0 \tag{A.2}$$

$$\varepsilon_g \frac{\partial c_3}{\partial t} + \frac{\partial N_3}{\partial y} = 0 \tag{A.3}$$

*Stefan–Maxwell equations*:

$$\frac{\varepsilon_g}{\tau^2}\frac{\partial x_1}{\partial y} = RT\left[\frac{x_1N_1 - x_1N_1}{p_c\mathscr{D}_{11}} + \frac{x_1N_2 - x_2N_1}{p_c\mathscr{D}_{12}} + \frac{x_1N_3 - x_3N_1}{p_c\mathscr{D}_{13}}\right] \tag{A.4}$$

$$\frac{\varepsilon_g}{\tau^2}\frac{\partial x^2}{\partial y} = RT\left[\frac{x_2N_1 - x_1N_2}{p_c\mathscr{D}_{12}} + \frac{x_2N_2 - x_2N_2}{p_c\mathscr{D}_{22}} + \frac{x_2N_3 - x_3N_2}{p_c\mathscr{D}_{23}}\right] \tag{A.5}$$

$$\frac{\varepsilon_g}{\tau^2}\frac{\partial x_2}{\partial y} = RT\left[\frac{x_3N_1 - x_1N_3}{p_c\mathscr{D}_{13}} + \frac{x_3N_2 - x_2N_3}{p_c\mathscr{D}_{23}} + \frac{x_3N_3 - x_3N_3}{p_c\mathscr{D}_{33}}\right] \tag{A.6}$$

in which

$$c_i = \frac{p_i}{RT} \tag{A.7}$$

$$x_i = \frac{p_i}{p_c} \tag{A.8}$$

Table 5
Critical properties of oxygen, water vapour and nitrogen

| Subscript | Species | $M$ | $T_c$ (K) | $p_c$ (bar) |
|---|---|---|---|---|
| 1 | $O_2$ | 31.999 | 154.35 | 50.40 |
| 2 | $H_2O$ | 18.015 | 647.30 | 221.2 |
| 3 | $N_2$ | 28.013 | 126.05 | 33.93 |

the subscripts 1, 2, and 3 in previous equations are related, respectively, to components oxygen, water vapour and nitrogen.

The pressure-diffusivity products (bar $cm^2/s$) are estimated [13] from critical temperature, critical pressure, and mass of the respective components (Table 5):

$$p\mathscr{D}_{12} = D_{12}(T) = 3.55\times10^{-4}\sqrt{\left(\frac{1}{M_1}+\frac{1}{M_2}\right)}\frac{(p_{c1}p_{c2})^{1/3}}{(T_{c1}T_{c2})^{0.750}}T^{2.334} = 4.281\times10^{-7}T^{2.334} \quad (A.9)$$

$$p\mathscr{D}_{13} = D_{13}(T) = 1.882\times10^{-3}\sqrt{\left(\frac{1}{M_1}+\frac{1}{M_3}\right)}\Big/(\sigma_{13}^2\Omega_{13})T^{3/2} = 5.338\times10^{-5}T^{1.5}/\exp\left(\frac{83.63}{T}\right) \quad (A.10)$$

$$p\mathscr{D}_{23} = D_{23}(T) = 3.687\times10^{-4}\sqrt{\left(\frac{1}{M_2}+\frac{1}{M_3}\right)}\frac{(p_{c2}p_{c3})^{1/3}}{(T_{c2}T_{c3})^{0.750}}T^{2.334} = 4.477\times10^{-7}T^{2.334} \quad (A.11)$$

A comparison of (A.9) and (A.11) yields $D_{23} \cong D_{12}$ ($D_{23}/D_{12} = 1.046$); for sake of simplicity, in this work the following is assumed:

$$D_{23} = D_{12} \quad (A.12)$$

As reported in Section 2.3 the water vapour contained in the gas reactants is considered in equilibrium with the surrounding liquid phase, and its saturation pressure $p_{sat}$ used here was fitted to the following expression according to tabulated values in [19]:

$$p_{sat}(T)(\text{bar}) = A\exp\left(-\frac{B}{T}\right) = 7.714\times10^5\exp\left(-\frac{5052.9}{T}\right). \quad (A.13)$$

Using the assumptions 3 and 4 in Section 2.3 and the Eqs. (A.7), (A.8) and (A.12) yields relatively at Eqs. (A.2) and (A.5)

$$\frac{\partial N_2}{\partial y} = 0 \quad (A.14)$$

$$N_2 = N_2(t) = \frac{p_2}{p_c - p_2}[N_1(y,t) + N_3(y,t)] \quad (A.15)$$

At diffusion layer/catalyst layer interface (Fig. 1, $y = L_d$) it is assumed that the instantaneous oxygen flux is equal to total oxygen flux consumed in catalyst layer:

$$N_1(L_d,t) = N_{1dc} = \frac{j_r}{4F} \quad (A.16)$$

the oxygen storage in catalyst layer is considered negligible.

As nitrogen is inert and its solubility in water is very little it is assumed that the Nitrogen flux in $y = L_d$ is null:

$$N_3(L_d,t) = 0. \quad (A.17)$$

Then using Eqs. (A.16) and (A.17) the Eq. (A.15) can be written as

$$N_2 = N_2(t) = \frac{p_2}{p_c - p_2}\frac{j_r}{4F}. \quad (A.18)$$

Substituting the Eq. (A.18) in Eq. (A.4), deriving the resulting equation with respect to $y$ and combining the result with Eq. (A.1) the following single partial differential equation is obtained

$$\frac{\partial p_1}{\partial t} = \omega\frac{\partial^2 p_1}{\partial \xi^2} - \psi\frac{j_r}{4F}\frac{\partial p_1}{\partial \xi} \quad (A.19)$$

in which $\xi$ is the dimensionless distance $y/L_d$ and

$$\omega = \frac{1}{\tau^2 L_d^2(p_2/D_{12} + (p_c - p_2)/D_{13})} = \frac{1}{\tau^2 L_d^2(p_{sat}/D_{12} + (p_c - p_{sat})/D_{13})} \quad (A.20)$$

$$\psi = \frac{RT}{\varepsilon_g L_d(p_c - p_2)} = \frac{RT}{\varepsilon_g L_d(p_c - p_{sat})}. \quad (A.21)$$

To solve the partial differential Eq. (A.19) it is necessary to define two *boundary conditions*. At flow channels/diffusion layer interface (Fig. 1, $y = 0$) the condition

$$p_1(0,t) = p_{1o} = \frac{p_c - p_{sat}}{1+\beta} = \text{constant} \quad (A.22)$$

applies, assuming constant oxygen partial pressure in flow channels. The parameter $\beta$ is the nitrogen-oxygen mole ratio of inlet air.

The second boundary condition is obtained evaluating the Eq. (A.4) in $\xi = 1$ and using the conditions (A.16), (A.17) and (A.18):

$$\frac{\partial p_1}{\partial \xi}(1,t) = \frac{\psi}{\omega}\frac{j_r}{4F}[p_1(1,t) + p_{sat} - p_c] \quad (A.23)$$

## References


[1] A. Parthasarathy, C.R. Martin, S. Snirivasan, A.J. Appleby, J. Electrochem. Soc. 139 (1992) 2530.
[2] D.B. Sepa, M.V. Vojnovic, M. Vracar, A. Damjanovic, Electrochim. Acta 32 (1987) 129.
[3] M. Uchida, Y. Aoyama, N. Eda, A. Ohta, J. Electrochem. Soc. 142 (1995) 4143.
[4] K. Broka, P. Ekdunge, J. Appl. Electrochem. 27 (1997) 281.
[5] D.M. Bernardi, M.W. Verbrugge, AIChE J. 37 (8) (1991) 1151.
[6] D.M. Bernardi, M.W. Verbrugge, J. Electrochem. Soc. 139 (1992) 2477.
[7] T.E. Springer, M.S. Wilson, S. Gottesfeld, J. Electrochem. Soc. 140 (1993) 3513.
[8] T.E. Springer, T.A. Zawodzinski, S. Gottesfeld, J. Electrochem. Soc. 138 (1991) 2334.

[9] Y.W. Rho, S. Snirivasan, J. Electrochem. Soc. 141 (1994) 2089.
[10] J.C. Amphlett, R.M. Baumert, B.A. Peppley, P.R. Roberge, J. Electrochem. Soc. 142 (1995) 1.
[11] D. Bevers, M. Wohr, K. Yasuda, K. Oguro, J. Appl. Electrochem. 27 (1997) 1254.
[12] C. Marr, X. Li, J. Power Sources 77 (1999) 17.
[13] R.B. Bird, W.E. Stewart, E.N. Lightfoot, Transport Phenomena, Wiley, New York, 1960.
[14] M.S. Wilson, J.A. Valerio, S. Gottesfeld, Electrochim. Acta 40 (1995) 355.
[15] T.E. Springer, T.A. Zawodzinski, J. Davey, R. Jestel, C. Lopez, J. Valerio, S. Gottesfeld, J. Electrochem. Soc. 140 (1993) 1981.
[16] T.E. Springer, T.A. Zawodzinski, M.S. Wilson, S. Gottesfeld, J. Electrochem. Soc. 143 (1996) 587.
[17] P. Bolognesi, V. Conte, G. Lo Bianco, M. Pasquali: Hy-sim: a modular simulator for hybrid-electric vehicles, in: Proceedings of the 18th International Electric Vehicle Symposium, EVS18, October 2001, Berlin, Germany.
[18] J.C. Amphlett, E.K. De Oliveira, R.F. Mann, P.R. Roberge, A. Rodrigues, J.P. Salvador, J. Power Sources 65 (1997) 173.
[19] K. Raznjevic, TOPLINSKE TABLICE I DIJAGRAMI, Tehnicka Knjiga, Zagreb, 1964.
[20] M. Eikerling, Y.I. Kharkats, A.A. Kornyshev, Y.M. Volfkovich, J. Electrochem. Soc. 145 (1998) 2684.
[21] T. Okada, G. Xie, M. Meeg, Electrochim. Acta 43 (1998) 2141.
[22] Y. Sone, P. Ekdunge, D. Simonsson, J. Electrochem. Soc. 143 (1996) 1254.
[23] J. Kim, S.M. Lee, S. Srinivasan, J. Electrochem. Soc. 142 (1995) 2670.
[24] V.A. Paganin, E.A. Ticianelli, E.R. Gonzalez, J. Appl. Electrochem. 26 (1996) 297.
[25] G. Squadrito, G. Maggio, E. Passalacqua, F. Lufrano, A. Patti, J. Appl. Electrochem. 29 (1999) 1449.